Batteries & Supercaps

Research Article
doi.org/10.1002/batt.202200010

Chemistry Europe
European Chemical Societies Publishing

www.batteries-supercaps.org

Clarification on the Gassing Behavior of Carbon-Coated $Li_4Ti_5O_{12}$ at Elevated Temperature: Importance of Coating Coverage

Kaviarasan Govindarajan,[a] Ralph Nicolai Nasara,*[b] and Shih-kang Lin*[a, c, d, e]

Lithium-ion batteries (LIBs) have become vital energy-storage devices in electric vehicles (EVs). $Li_4Ti_5O_{12}$ (LTO) is a promising material of LIB because of its high rate capability, cyclability, and safety compared to the graphite-based anode materials in commercial LIBs. However, one of the major concerns in LTO-based LIBs is gassing, which results from the interfacial reaction between LTO and organic electrolyte solutions, unlike the reduction decomposition of an electrolyte in graphite electrodes. Carbon coating on LTO has been proposed to mitigate the gassing by preventing such side reactions, even though reports have been conflicting. In this work, there are different kinds of carbon-coated LTO deposited using the thermal decomposition of ethanol that has been investigated at elevated temperature using *In Operando* pressure analysis to answer the paradox of the effect of carbon coating on the gassing behavior on LTO. Our Spatial Raman Spectroscopy Analysis (SRS) shows that the carbon coating coverage is likely responsible for the discrepancy in the gassing behavior reported by other studies. Our proposed deposition process achieves complete coverage with an ultrathin 3 nm carbon coating layer which mitigates the interfacial reactions while improving electrochemical performance.

Introduction

Globally, the concern for the environment is rising due to increased air pollution, leading to a climate crisis. One of the major air pollution causes is the automotive sector, which contributes between 15% and 25% of polluting emissions.[1] Electric vehicles (EVs) that replace conventional internal combustion engines with electric motors can help reduce air pollution from the automotive sector. Currently, Lithium-ion batteries (LIBs) are the widely used energy storage systems for EVs because it has a high energy density and comparable power density among other energy storage systems. Despite many advantages, a few issues need to be addressed with the current commercial LIBs. Current LIBs face challenges such as poor rate capability, poor cycle life, and safety concerns because of the intrinsic limitations of the anode material, which has popularly been Graphite. It is essential to develop anode materials with fast-charging capabilities. There are active research and developments for commonly used LIB anodes such as Graphite and Si to meet the requirements for fast charging. As an alternative to these high-capacity and high-current density anode materials,[2] which have been viewed as promising materials to work in post-LIB systems such as sodium-ion batteries,[3] Potassium-ion batteries,[4] and Zinc-ion batteries.[5,6] $Li_4Ti_5O_{12}$-based LIBs (LTO) are proven to achieve EVs' standard requirements.[7] LTO is a promising anode material that can replace graphite to overcome these issues in LIBs. With its high working voltage (~1.55 V vs. Li^+/Li), which practically eliminates the threat of dendrite formation and nearly zero percent of volume expansion, the use of LTO as anode material enhances the device's safety while offering fast-charging capabilities.

However, gassing is one of the serious issues in batteries at elevated temperatures. Over the years, there have been many publications on the gassing behavior of LTO based LIBs, which shows the keen importance of LTO electrodes on EV application.[8–13] LTO based LIBs gassing is much more severe, which limits the usage of LTO, despite its advantage for EV applications. In graphite-based LIBs, electrolyte decomposes during the initial cycle and forms a stable solid electrolyte interphase (SEI) layer.[14] This SEI layer blocks the further decomposition of the electrolyte. In LTO, there is no such SEI formation because its high working voltage ~1.55 V vs. Li/Li^+ is above the conventional electrolyte decomposition potential.[15] Unlike graphite, the electrolyte decomposition in LTO is due to

[a] K. Govindarajan, Prof. S.-k. Lin
Department of Materials Science and Engineering
National Cheng Kung University
Tainan 70101, Taiwan
E-mail: linsk@mail.edu.ncku.tw
[b] Dr. R. N. Nasara
Graduate School of Engineering
Kyoto University
Kyoto 615-8510, Japan
E-mail: nasara.ralphnicolai.3s@kyoto-u.ac.jp
[c] Prof. S.-k. Lin
Hierarchical Green-Energy Materials (Hi-GEM) Research Center
National Cheng Kung University
Tainan 70101, Taiwan
[d] Prof. S.-k. Lin
Program on Smart and Sustainable Manufacturing Academy
of Innovative Semiconductor and Sustainable Manufacturing
National Cheng Kung University
Tainan 70101, Taiwan
[e] Prof. S.-k. Lin
Core Facility Center
National Cheng Kung University
Tainan 70101, Taiwan

Supporting information for this article is available on the WWW under https://doi.org/10.1002/batt.202200010

the interfacial reaction between electrolyte and LTO surface. The electrolyte decomposition is spontaneous, and the decomposition products on the surface of LTO are gradually generated as various gases. The various gas generation reactions were proposed over the years in the literature.[16-.18] The reported gases in the literature are H_2, CO_2, CO, CH_4, C_2H_4, C_2H_6, C_3H_6, and C_3H_8,[19] among which H_2 is the major gas evolved.

Wu et al.[20] investigated the spinel LTO electrode using electrochemical impedance spectroscopy (EIS) measurements during the first charge-discharge cycle. They believed that the charging between 1.55–1.75 V *vs.* Li^+/Li induces H_2 evolution on the LTO surface by the reduction of absorbed hydroxyl group through electron transfer reactions. He et al.[16] proposed that gasses like H_2, CO_2, and CO were generated from the interfacial reaction, which involves phase change of LTO (111) to (222) on the surface and removal of terminating ions on (111) facet of LTO such as Li^+ and O^{2-}. He et al.[21] investigated LTO half-cells using *in-situ pressure* and online electrochemical mass spectrometry (OEMS) to analyze the generated gases. They found that, during the first discharge, most of the detected H_2 gas was due to the presence of trace amounts of water and was not observed in subsequent cycles. Also, CO_2 was originated from several reactions, such as the decomposition of the carbonates initiated by the presence of Ti^{4+} on the LTO surface. Qin et al.[18] proposed a hydrogen release reaction at the surface of fully charged LTO. Initially, the electrolyte solvent is electrostatically attracted on the surface of fully charged LTO, after which the breakdown of the hydroxyl group leads to the release of H_2 gas. The chemical reduction reaction occurs on the surface of fully charged LTO stored at 55 °C. These studies effectively show that the gas evolution reactions are continuous and do not self-terminate in LTO-based LIBs.[16,22]

The LTO surface mainly commences the gassing reactions in either cycling or fully charged storage conditions at both elevated and room temperature, so avoiding the contact between LTO surface and electrolyte has been reported as an effective strategy. Surface coating layers such as carbon,[16,23] ZnO,[24] AlF_3,[25] polyamide[26] and SEI layers[27,28] are most commonly used as protective layers for gassing reactions. Among the proposed coating layers, carbon proves to be advantageous because it further improves the electronic conduction, which significantly improves the electrochemical performance.[29,30] He et al.[31] coated LTO with an amorphous carbon coating to form the SEI layer. The SEI layer was formed during the first cycle while cycling in the range of 2.5–0 V, after which further decomposition of electrolyte was suppressed. He et al.[16] compared the gassing behavior of uncoated and carbon-coated LTO (LTO/C) and prepared a soft-packed battery using $LiNi_{0.33}Mn_{0.33}Co_{0.33}O_2$ cathode material. The full-cell batteries were tested in different conditions, and unlike the battery containing the uncoated LTO, the batteries containing the LTO/C showed no swelling.

Similarly, Wen et al.[23] also studied the carbon-coated LTO and uncoated LTO batteries instead of a $LiMn_2O_4$ cathode material. The batteries were tested for 1000 cycles, and they had found that the carbon coating on the LTO can suppress the gassing behavior. Their proposed reason for the facilitated gassing reactions was the high reactivity of carbon coatings at elevated temperatures. The studies mentioned above showcased that the carbon coating on LTO can mitigate the gassing at room temperature. However, at an elevated temperature of 50 °C, He et al.[21] studied the gas evolution of uncoated, carbon-coated, and ceramic-coated LTO with different electrolytes using *in-situ pressure* analysis. They showed that the carbon coating layers on the LTO surface promote the gassing behavior instead of suppressing it, a controversial conclusion from the literature above.

This study briefly clarifies such a controversial conclusion about the surface modification using carbon on the LTO and its gassing behavior. In this work, different kinds of carbon-coated LTO was deposited using the thermal decomposition of ethanol were investigated at elevated temperature using *in operando* pressure analysis to answer the paradox of the effect of carbon coating on the gassing behavior on LTO at an elevated temperature. Here we report that the carbon coating coverage has a polarizing impact on the gassing behavior of carbon-coated LTO. Finally, our optimized carbon deposition process resulted in an ultrathin 3 nm conformal carbon coating layer which significantly suppressed gassing while significantly enhancing rate capability.

Experimental Section

Materials preparation

Commercial LTO (cLTO) purchased from MSE supplies LLC is thoroughly mixed with ethanol (98% purity) in the ratio of 1:1.5 [LTO(g): ethanol(mL)]. The mixture is transferred to Swagelok stainless steel reactors. The reactor is heated at 800 °C in different durations (1, 2, and 3 h) with a heating rate of 5 °C per minute in H_2 (10%)/N_2 (90%), reducing atmosphere and allowed to cool at a room temperature after the reaction. The high-purity ethanol gradually evaporates at around 80 °C, and the gaseous phase forms inside the reactor vessel. In high temperatures, high autogenic pressure was induced inside the vessel, which facilitates the carbon deposition on the surface of the LTO. For further information, please refer to the article.[32] The carbon-coated samples with 1, 2, and 3 h process duration are labelled as LTO/C-1 h, LTO/C-2 h, and LTO/C-3 h, respectively.

Characterization techniques

The powders were analyzed using Bruker D2 Phaser with Cu K_α (0.15405 nm) source and 1D LYNXEYE detector at an operating voltage of 30 kV and $\pm 0.02°$ accuracy. The diffraction patterns were recorded from 10° to 80° diffraction angle, at a scan rate of 2°/min. The Raman spectra were acquired using UniDRON Raman Spectrometer. The samples were exposed to a 532 nm laser using a 100× lens with NA = 0.8. The lowest laser power (1%) possible with an exposure time of 15 s was used to minimize the laser-induced sample heating. High-resolution transmission electron microscopy (HRTEM) images and selected area diffraction pattern (SAED) were eventually captured using JEOL JEM-2100F with a spherical aberration (Cs) corrector. The electrochemical performances were measured using Biologic VSP. The pressure and temperature

profiles were recorded using EL-CELL (PAT-CELL-Gas) and controlled by biologic SP-300. The electronic conductivity was measured using the four-point probe method (Keithley's Standard Series 2400 Source Measure Unit) with the Napson probe, and a constant current of 100 mA is applied to measure the resistance.

Electrode and coin cell preparation

The electrodes were prepared with 80:10:10 weight ratio of active material: Super-P carbon (conductive additive): Polyvinylidene difluoride (PVDF) binder by beginning to mix the active material conductive carbon through ball-milling at 600 rpm for 3 h. Then the premixed PVDF and N-Methyl-2-pyrrolidone (NMP) mixture was added on, and the mixture was ball-milled for 30mins to form a slurry. The slurry was coated with copper foil using a doctor blade and dried in a vacuum oven for 12 h at 120 °C. The electrodes were cut into discs of 13 mm diameter. Electrochemical characterization of electrode materials has been investigated using CR-2032-coin cells with the lithium metal counter electrode, 1 mol $LiPF_6$ in EC: DEC (1:1 volume ratio) electrolyte, Celgard 2400 separator, and synthesized materials coated on current collector served as working electrodes. The coin cell was assembled inside an Ar-filled glove box with O_2 and H_2O levels of <0.5 ppm.

In operando pressure measurement

Pressure cell (EL-CELL, PAT-CELL-Gas) was mainly used to perform potential dependent pressure and temperature analysis. The cell was assembled inside an Ar-filled glove box in a three-electrode setup with lithium metal as counter and reference electrode. The areal mass loading of the working electrode was approximately 7.5 mg/cm^2 (~0.1 mg difference between materials) with an active material loading of 8 mg approximately. The 7.5 mg/cm^2 loading area employed in this study is higher than most of the LTO gassing-related research (6.25 ± 0.15 mg/cm^2,[17] 5 mg/cm^2[21]) and relevant to that of LTO electrodes found in commercial-level batteries {300 mAh pouch cell with 5.3 mg/cm^2 coating weight[12]}. Therefore, the results provided in these studies are commercially relevant, and we recommend that future studies be implemented on this level of commercial loading. 1 M $LiPF_6$ in Ethylene Carbonate: Diethylene Carbonate (1:1 volume ratio) mixture was used as an electrolyte with poly (ether-ether-ketone) (PEEK) separator.

Results and Discussion

Influence of carbon coating on the gassing behavior of LTO

To compare the gassing behavior, the pressure cell was assembled and cycled at 0.1 C -rate between 1 and 2.5 V vs. Li/Li^+ for cLTO, LTO/C-1 h, and LTO/C-3 h at room temperature. In Figure 1, the green curve (dash) corresponds to Potential vs. Time, whereas the blue curve (dash-dot) indicates Temperature vs. Time, and the red curve (straight) indicates Pressure *vs.* Time. We can clearly understand that there is no significant change in the cell pressure while cycling it at room temperature (Figure 1a–c), which agrees with many reported works on gassing.[16,18] Literature defined the mitigation of gassing using the carbon coating after testing for many cycles or storage over a period of time.[16,23] This shows that the gassing rate is slow at room temperature, so no gassing is observed during the experiment's initial cycles. The original pressure value from the cell is around 1 bar. The pressure values are normalized to an initial value of zero to get a clear view of the pressure change.

A systematic calibration has been performed to accurately analyze and attribute the source of the generated gaseous species. The generation of gaseous species can be initiated by any such components inside the pressure cell (Figure S1). To exclude the influence of the pressure cell components, we assembled the cell without any electrodes and only with the addition of the electrolyte on the separator. The cell temperature was raised to 55 °C and was maintained for more than 30 h; then, the cell was allowed to cool down (Figure S2). The observed potential is due to the lithium metal reference in the insulation sleeve (three-electrode assembly setup), and cell pressure gradually increases due to the rise in the cell temperature. There is no further increase in the cell pressure, which verifies that the components do not play any role in generating gaseous species.

Later, the pressure cell is assembled for cLTO, which was tested at 55 °C and galvanostatically charged at a C/5 rate. To understand the gassing behavior, the potential/pressure profile is divided into four regions based on the possible generation of gaseous species (Figure 1d):

Region 1 is the equilibrium period of 10 hours. During the equilibrium time, the cell's temperature is raised to 55 °C and maintained. The rapid rise in the internal pressure of the cell is solely due to the cell's temperature increase which can be defined by the ratio of the number of moles in the ideal gas Equation (1):

$$\frac{P_1V_1}{P_2V_2} = \frac{n_1RT_1}{n_2RT_2} \quad (1)$$

where V is the cell volume, V_1 and V_2 should be the same. The ratio of the number of moles, $\frac{n2}{n1} = \frac{P2\ T1}{P1\ T2} = \frac{1.11\times303.06}{1.019\times328.75} = 1.007$, shows that the number of moles is the same in the initial and end equilibrium period. Therefore, no gas generation was observed during the resting period of 10 h to attain equilibrium.

Region 2 is the initiation of galvanostatic discharging (until the ~1.55 V plateau), the sudden increase in the pressure has been attributed to H_2 and CO_2 evolution. The possible net reactions involve the electrochemical reduction of impurities such as water: as contamination in the electrolyte, and as trace amounts of moisture within the electrochemical cell (where the Li in lithiated $Li_7Ti_5O_{12}$ reacts with water to form delithiated $Li_4Ti_5O_{12}$) and along with residual hydroxyl groups on the surface of LTO, such reactions have been proposed to lead to a greater gas generation source for H_2 evolution,[12,17,33–35] while the trace amounts of water and its by-products from the initial electrochemical reduction may also play a role in subsequent/parallel reactions that release CO_2 gas.[17,36,37]

Region 3 is the lithiation of bulk LTO and delithiation until ~1.55 V plateau, which is a two-phase separation mechanism with the coexistence of $Li_4Ti_5O_{12}$ (Ti^{4+}) and $Li_7Ti_5O_{12}$ (Ti^{3+}). In line with a particle-particle reaction mechanism, it is proposed that the surface layer of the insulating LTO should be lithiated first

Research Article
doi.org/10.1002/batt.202200010
Chemistry Europe
European Chemical Societies Publishing

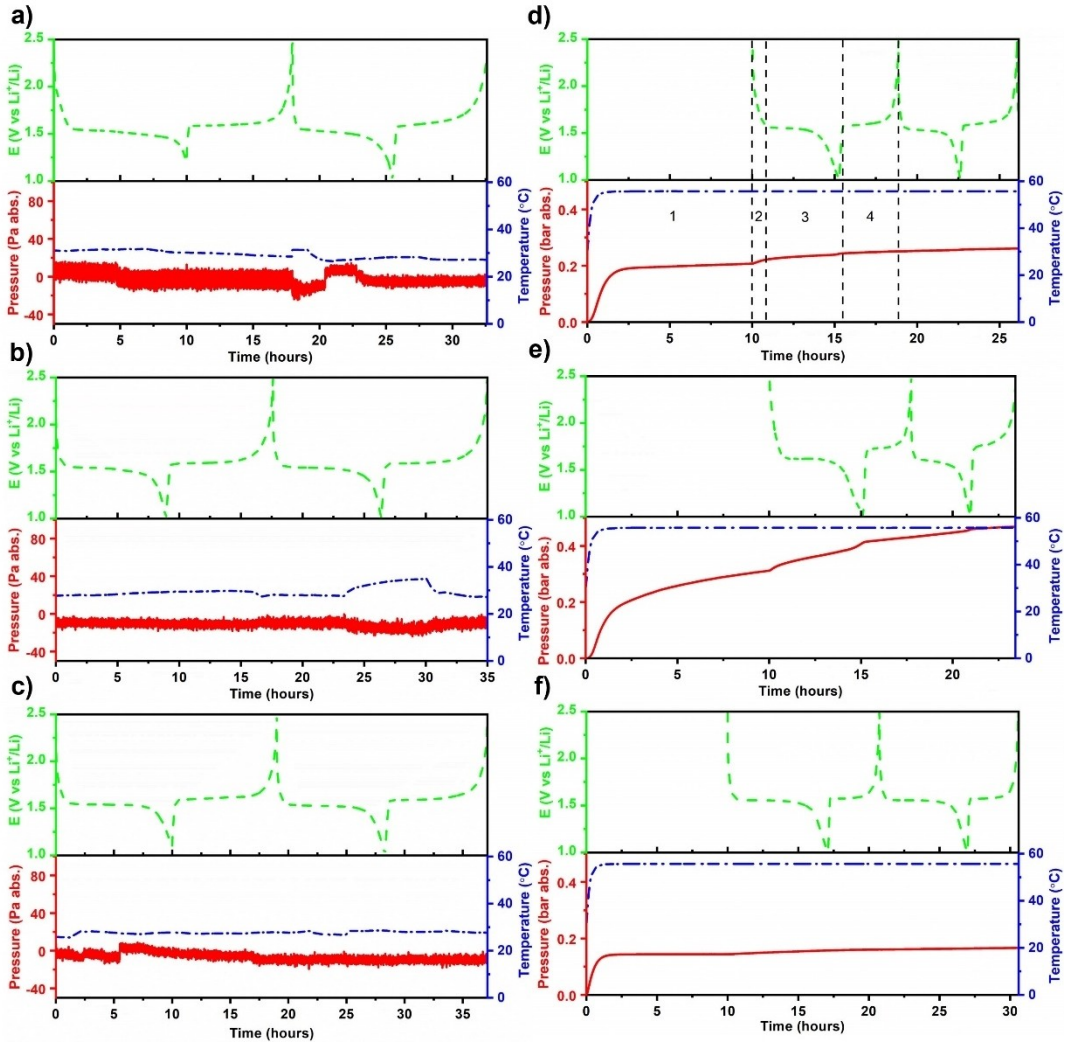

Figure 1. The first two galvanostatic cycles of a) cLTO, b) LTO/C-1 h and c) LTO/C-3 h at C/10 at room temperature (pressure in Pa, 1 Pa = 1.0E^{-5} bar) and d) cLTO, e) LTO/C-1 h and f) LTO/C-3 h at C/5 at 55 °C (pressure in bar).

because this is where the charge-transfer reaction ($Li^+ + e^- + Ti^{4+} \rightarrow Li^+ + Ti^{3+}$) occurs.[38,39] This indicates that $Li_7Ti_5O_{12}$ (Ti^{3+}) is present at the particle boundary or the outermost surface/shell during lithiation and that Li-insertion progresses inside each particle, moving toward the core. This core-shell model has been extensively captured with *ab initio* modelling[40] and resolved in real-space distribution.[41,42]

Region 4 is the delithiation process of the charged LTO. The delithiation process changes $Li_7Ti_5O_{12}$ to $Li_4Ti_5O_{12}$, where Ti^{3+} releases an electron to the outer circuit and reverts to Ti^{4+}. The decreased ratio of Ti^{3+}/Ti^{4+} is responsible for the small pressure change during the delithiation process compared to the lithiation process.[21,43] Our analysis reveals that during the delithiation process at Region 3, the (*dP/dt*) value is 23 mbar/min g, which is one order of magnitude less than that of Region 1 with a (*dP/dt*) value of 152 mbar/(min g). He et al. investigated the gassing behavior of LTO at elevated temperatures using a similarly configured electrochemical pressure test cell. They reported that measurement that at this region, the gas evolution rate is constant at ~2 mbar/(min g) whereas during the start of the galvanostatic discharging (Region 1) the gas evolution rate was as high as ~30 mbar/(min g).[21]

Therefore, the obtained pressure change is quantitatively smaller than lithiation due to the decreased Ti^{3+}/Ti^{4+} ratio. The pressure change difference can be rationalized by the catalytic role of Ti^{3+} in gassing-induced reactions,[44] the decreased Ti^{3+}/Ti^{4+} ratio changes the Ti-atom distribution in the surface layers; effectively altering the number of structural defects such as electronic holes,[43] which can act as electron capturing and releasing centers can manipulate the catalytic capability.[37] This proposed phenomenon is a possible reaction for CO_2 gas generation and links the difference in the equilibria of the Ti^{3+}/Ti^{4+} species and the perceived specific pressure increase rate. The delithiation also shows similar pressure change to lithiation, but the rate at which the pressure changes is comparatively lower than lithiation, which agrees with the literature that gassing is severe during lithiation compared to delithiation, particularly in the first few cycles.[16] The second possibility is that the decomposition of electrolyte solvent during the first lithiation leaves the decomposed products on

Research Article
doi.org/10.1002/batt.202200010
Chemistry Europe
European Chemical Societies Publishing

the surface of the LTO, which acts as a partial passivation layer to mitigate the gassing reaction. This partial layer is responsible for the reduced gassing rate in the subsequent cycle, compared to the first lithiation.[45]

The previously reported literature suggests that the protective coating layers on the LTO surface can help to mitigate the gassing.[16,23] Contradictory, our results show that the carbon-coated LTO, specifically LTO/C-1 h, shows severe gassing behavior at elevated temperature as shown in Figure 1(e), which agrees with He et al.[21] The pressure generated in the LTO/C-1 h cell is approximately twice that of cLTO, but less or almost no gassing in the LTO/C-3 h cell (Figure 1f). The paradox can be explained by the carbon coating coverage resulting from the varied duration of the deposition process. Ti^{3+} on the surface of the LTO acts as a catalyst to promote the interfacial reactions on the bare LTO surface, whereas the carbon coating on the LTO surface prevents such interfacial reactions to mitigate the gassing. Yet, a possibly partial carbon-coated LTO (for this case, LTO/C-1 h) has promoted the gassing of LTO. The promotion of gassing in LTO/C-1 h can be explained in a viewpoint that increased electron conductivity of the LTO leads to improved electron conduction paths.[46–48] The electronic conductivity, shown in Figure 2(a) is measured for the working electrodes coated on the copper foil, and the conductivity is calculated using the resistance value from the four-point probe method. The conductivity of cLTO is the order of 10^{-6} S/cm, which is more than the normal value reported in the literature. The increased value is due to conductive additives in the working electrode. The conductivity is increased to 10^{-4} S/cm for LTO/C-1 h and 10^{-3} S/cm for LTO/C-3 h because of the carbon coating on the surface. From the hypothesized gassing reactions, it is clear that the surface reactions need electrons to release gaseous products.[16,20,49] An abundance of free electrons can be perceived, where the LTO/C-3 h has a higher electronic conductivity than that of LTO/C-1 h. In the case of a partially coated surface, the facilitated electron conduction path serves as a free electron "pool" where spontaneous charge-transfer of electrons to non-coated active sites promotes gassing-related chemical reactions occurring at the electrode-electrolyte interface, resulting in accelerated gas generation. Whereas an arguably similar or even abundant electron pool is present for LTO/C-3 h, the full passivation by conformal carbon coating limits the charge-transfer reaction involving oxidizing/reducing the organic molecules in the electrolyte.

This is evident with the increase in pressure change being the lowest for LTO/C-3 h, which is completely carbon-coated LTO, compared to bare and partially carbon-coated. So, the complete carbon coating coverage on LTO can help us reduce the gassing considerably by simply passivating the electrode and electrolyte interface. The combined internal pressure shows us the importance of conformal coating on the LTO (Figure 2b). A schematic representation of the proposed surface behavior is shown in Figure 2(c). The following section will elucidate advanced materials characterization of the coating quality, coverage, and insights on defect density induced by the carbon deposition.

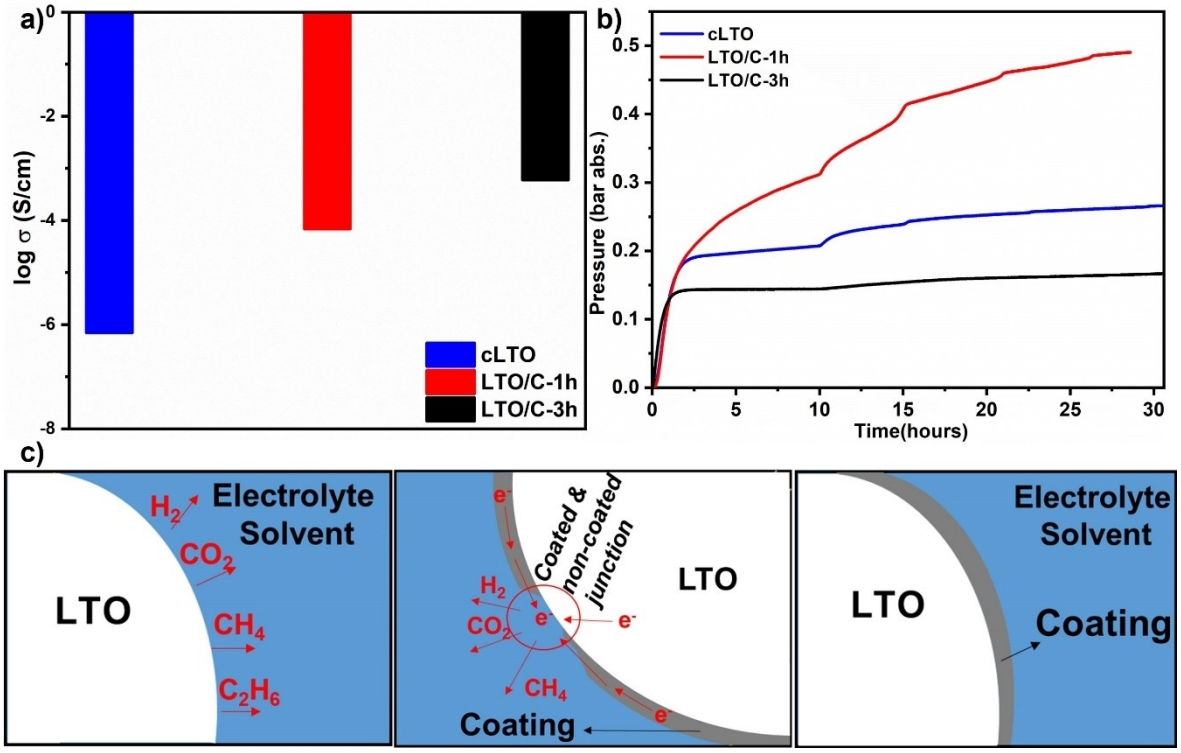

Figure 2. a) Electrical conductivity of cLTO, LTO/C-1 h, and LTO/C-3 h, b) pressure analysis at 55 °C of bare, partially coated, and completely coated surface, and c) schematic representation of proposed surface behavior.

Research Article
doi.org/10.1002/batt.202200010
Chemistry Europe
European Chemical Societies Publishing

Analysis of the surface coating

XRD pattern of LTO/C-1 h and LTO/C-3 h consists of all peaks corresponding to LTO (JCPDS No. 49-0207), as which the structure of the LTO was not affected by the coating process, despite its high temperature and high pressure (Figure 3a). The magnified image of the 111 peak (Figure 3b) shows a shift in LTO/C-3 h due to the oxygen vacancy. Since the coating process takes place in a reducing atmosphere, which is also favorable for oxygen vacancy formation on the surface of the LTO.[32,50,51] The Raman spectra of LTO contains a set of six bands (Figure 3c) with major bands centered at 231 cm^{-1} (which is F_{2g} vibrations in TiO_6 octahedral), 341 cm^{-1} (F_{2g} vibrations in LiO_6 octahedral), 421 cm^{-1} (E_g vibrations in LiO_4 tetrahedral), and 668 cm^{-1} (A_{1g} vibrations in TiO_6 octahedral). In comparison, the two minor bands are located at 258 cm^{-1} (attributed to F_{2g} vibrations in TiO_6 octahedral) and 737 cm^{-1} (so-called A_{1g} shoulder). In addition to the bands mentioned above, two additional bands (D and G) were observed for LTO/C-1 h and LTO/C-3 h, indicating the successful deposition of carbon coating layers on the surface.

HRTEM image of the LTO/C-1 h particle (Figure 4a and b) shows that the carbon coating was not fully coated, and the thickness of the coating is very thin, approximately 0.8 nm (Figure 4b), leaving the possibility of some of the exposed LTO surface. On the other hand, the LTO/C-3 h particle (Figure 4c and d) is uniformly coated with an ultrathin layer (~3 nm) of carbon throughout the surface of the LTO (Figure 4d). The inset in Figure 4(a) shows the diffraction pattern of LTO. HRTEM will just allow us to examine and visualize qualitatively a highlighted area of the particle, which is indeed not sufficient to claim and quantify the efficacy of the carbon coverage. We have previously introduced that Raman spectroscopy (RS) is a facile and cost-effective tool that has been used for in-line quality control for the application of coating layers.[50,52,53] Spatial RS measurements (SRS) are measured to get 100 Raman spectra for each sample with a 1 μm step size in XY plane of 10 μm ×10 μm area to give localized information about the coating coverage on the surface the LTO. Instead of discussing just the intensity from carbon and LTO separately, the I_C/I_{LTO} ratio is used, which is the relative Raman intensity of the carbon layer. The relative Raman intensity will stop the problem from Raman intensity reduction by carbon layer and allow the clear differentiation of the coating difference on the surface. I_{LTO} and I_C are Raman spectra′ integral areas from 50 to 900 cm^{-1} for LTO intensity and 900 to 1800 cm^{-1} for carbon intensity.

For an in-depth insight into the application of SRS as an in-line quality control tool, the Raman spectra of commercial carbon-coated LTO (cLTO/C) are also included in this section of the study. The I_C/I_{LTO} ratio for the different materials is shown in Figure 5(a–d), and the ratio is shown to increase with the prolonged carbon deposition duration because the intensity of the Raman vibrations from the LTO is reduced by increased carbon coating thickness. The smaller I_C/I_{LTO} ratio distribution in LTO/C-1 h (Figure 5b) shows that the intensity of the Raman vibrations arising from carbon is significantly lesser than the intensity of Raman vibrations from the LTO, which means that coating thickness is very thin, also there may be a possibility of exposed LTO surface. In the case of cLTO/C (Figure 5a), the distribution is much smaller compared to LTO/C-1 h. This may be due to the un-uniform carbon coating, and severe agglomeration of carbon particles (similar to a composite physical mixture of carbon and LTO rather than a homogeneously deposited coating) are even imaged on selected particles that were viewed with HRTEM (Figure S3). Higher (1.7) and Lower value (0.6) I_C/I_{LTO} ratio in LTO/C-3 h (Figure 5d) ensures that all the LTO particles′ surface is completely covered with carbon coating. Since our XRD (Figure 3b) shows the presence of oxygen vacancy, and the HRTEM image (Figure 3c) shows that the coating is uniform for LTO/C-3 h. One possible way to intercept the broadened distribution of I_C/I_{LTO} ratio in LTO/C-3 h is due to the induced oxygen vacancy on the surface, other than the carbon coating non-uniformity, which also affects the Raman response from the LTO[50] (Figure S4). The structural heterogeneity of the carbon deposited on the surface of the LTO is important for the electrochemical performance of the materials. The structural heterogeneity of the coated carbon can be explained using I_D/I_G ratio (Figure 5e). The structural heterogeneity gradually decreases with the increased carbon coating thickness: cLTO/C and LTO/C-1 h show high structural heterogeneity over LTO/C-2 h and LTO/C-3 h. D band vs. G band position as shown in Figure 5(f). Band position is more dispersive for cLTO/C, which can correlate with structural heterogeneity and LTO/C-1 h. The position is compact for

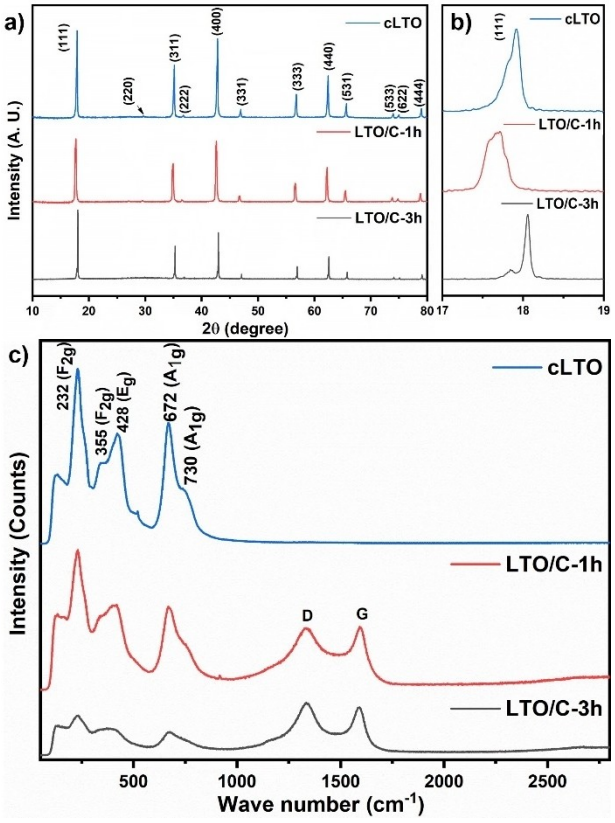

Figure 3. a) XRD pattern, b) magnified view of (111) peak, and c) Raman spectra of cLTO, LTO/C-1 h, and LTO/C-3 h.

Research Article
doi.org/10.1002/batt.202200010
Chemistry Europe
European Chemical Societies Publishing

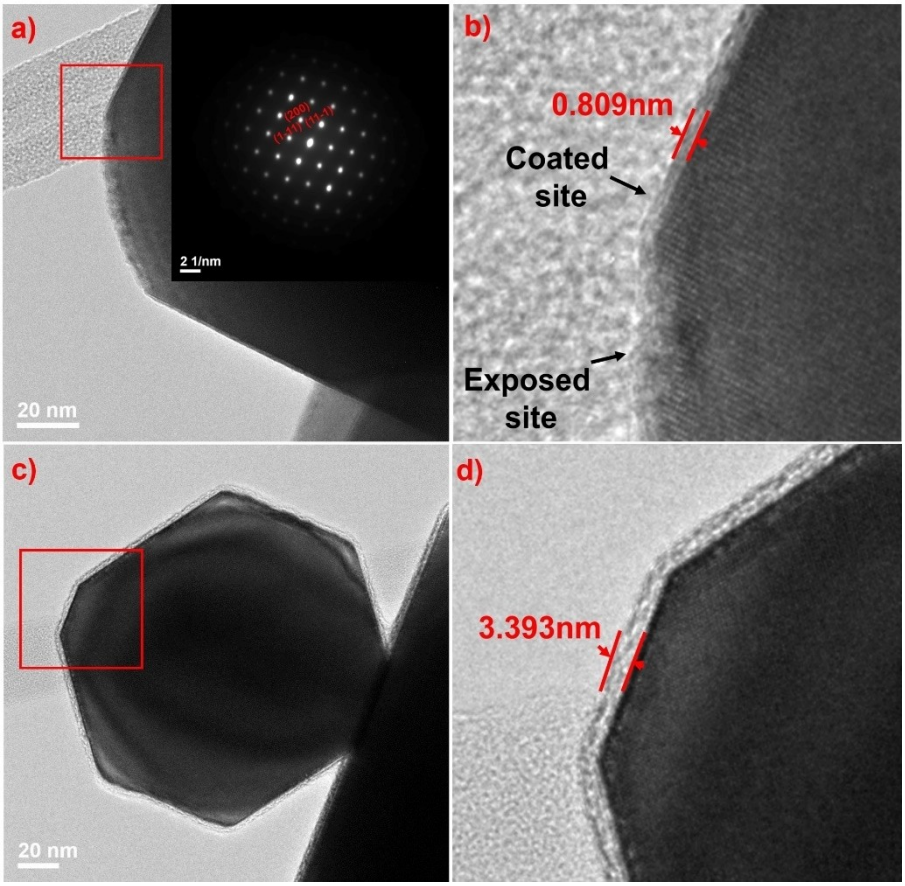

Figure 4. HRTEM images of a) LTO/C-1 h, c) LTO/C-3 h, magnified images of carbon coating on b) LTO/C-1 h surface, and d) LTO/C-3 h surface, respectively. Inset in a) is the SAED image.

increased coating time. The previous section shows how important the conformal coating is in the gassing behavior of LTO. SRS shows that our coating process yields uniform and conformal carbon coating on the surface of the LTO particles. SRS can be used as a preliminary check for carbon-coated materials since non-uniform coatings may affect the performances of the materials, especially at elevated temperatures.

Electrochemical performance

In addition to the mitigation of the gassing, carbon coating should also improve the electrochemical performance of the LTO, which is an ultimatum. The electrochemical performance of the cLTO, LTO/C-1 h, and LTO/C-3 h is discussed in the section. Figure 6(a) shows the cyclic voltammogram (CV) studies cycled at a scan rate of 0.1 mV/s between 1 and 2.5 V. From the cyclic voltammogram, we can observe a set of cathodic (1.48–1.51 V) and anodic peaks (1.63–1.67 V) corresponding to Li^+ intercalation and deintercalation, respectively. The sharper peaks indicate the improved kinetics in the carbon-coated LTO's electrodes. The ideal LTO system's CV curve should show symmetric oxidation and reduction peaks.[54] The asymmetric oxidation and reduction peaks, in our case, are because lithiation is the conversion of Ti^{4+} to Ti^{3+} from the surface to the bulk of the particle, forming a core-shell mechanism, whereas delithiation is a single-step conversion along with the whole particle.[38–42] Figure 6(b) shows the Specific capacity of cLTO, LTO/C-1 h, and LTO/C-3 h with some of the coated LTO (polyimide-modified LTO,[26] C-coated LTO,[55] C-coated LTO[56]) reported on the literature at various C-rates. The Specific capacity of LTO/C-3 h were 180, 174, 165, 157, 138, 113 and 81 mAh/g at 0.1, 0.2, 1, 2, 5, 10 and 20 C rates respectively, which is better compared to LTO/C-1 h and cLTO, whereas for LTO/C-1 h the values were 172, 161, 156, 147, 123, 96 and 73 mAh/g at 0.1, 0.2, 1, 2, 5, 10 and 20 C rates respectively and cLTO which were 160, 154, 145, 139, 119, 92 and 51 mAh/g at 0.1, 0.2, 1, 2, 5, 10 and 20 C rates respectively. The specific capacity values of Polyimide-modified LTO[26] are higher, but the synthesis method is quite complicated and costly. In contrast, our proposed carbon deposition method offers a route that is easier to scale up and economical to synthesize carbon-coated LTO with comparable performance. The rate capability of electrodes was shown in Figure 6(c), where five cycles were cycled in increasing current densities. The cLTO, LTO/C-1 h, and LTO/C-3 h electrodes displayed capacity retention of 31 %, 39 %, and 45 % at 20 C, corresponding to the capacity at 0.1 C, showing that the carbon coating on LTO improves the capacity retention of the LTO and also the Coulombic efficiency during initial cycles. Finally, LTO/C-3 h

Research Article
doi.org/10.1002/batt.202200010
Chemistry Europe
European Chemical Societies Publishing

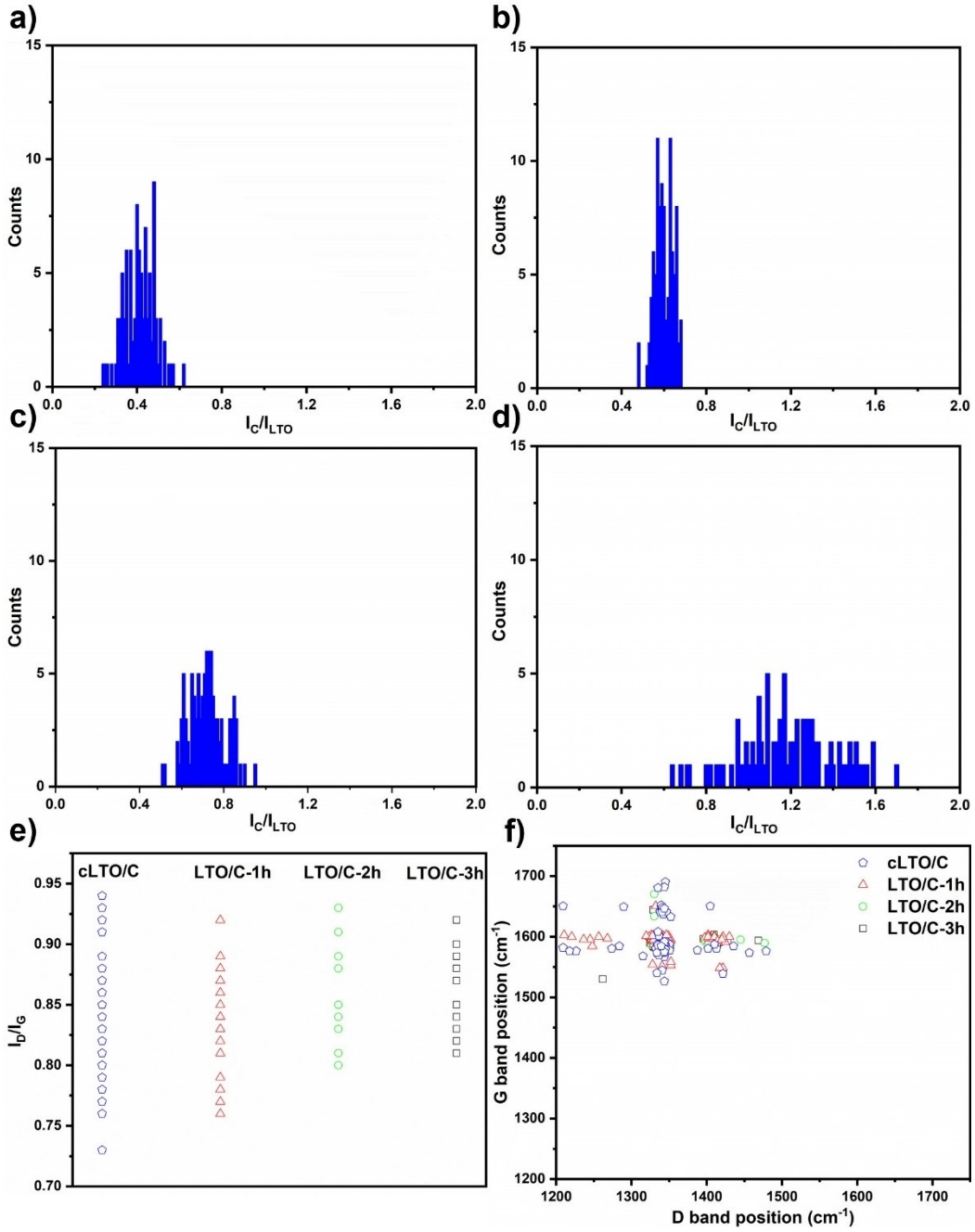

Figure 5. Histograms over 100 Raman spectra plotted for a) cLTO/C, b) LTO/C-1 h, c) LTO/C-2 h, and d) LTO/C-3 h, e) I_D/I_G ratio and f) D and G band position of cLTO/C, LTO/C-1 h, LTO/C-2 h and LTO/C-3 h respectively.

shows an excellent cycling performance than the cLTO at a 1 C rate for 200 cycles. The ultra-thin carbon coating applied in the LTO/C-3 h resulted in a significant increase of up to 20 mAh/g in utilizable specific capacity at 1 C-rate and retained 98% of its initial capacity after 200 cycles. Furthermore, the LTO/C-3 h has an average Coulombic efficiency of 99.99% is characteristic of an excellent and stable electrochemical performance. (Figure 6d). Our simple and economical carbon process achieved conformal carbon coating on the LTO surface, which enhances the electrochemical performances of the material.

Conclusion

Gassing behavior of pristine and carbon-coated LTO was investigated by *In Operando* pressure and temperature measurements, both at the room and elevated temperatures. The surface coating quality and coverage difference significantly affect the gassing behavior. No pressure change was observed in the electrochemical cell at room temperature, but at elevated temperature, the internal pressure developed in the partially carbon-coated LTO/C-1 h is twice that of the pristine LTO, which shows the importance of coverage efficiency on the

Research Article
doi.org/10.1002/batt.202200010

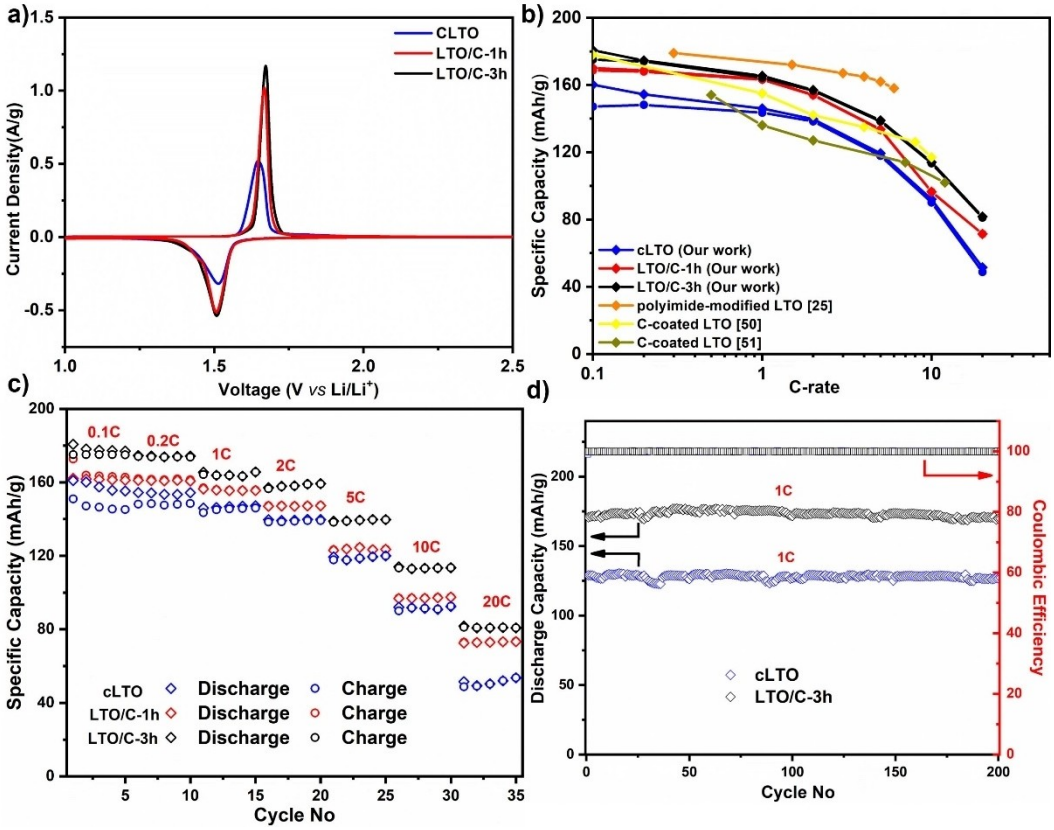

Figure 6. a) Cyclic voltammogram and b) specific capacity of cLTO, LTO/C-1 h and LTO/C-3 h at various C-rates, and benchmarking with other coatings. c) Rate capability of cLTO, LTO/C-1 h, and LTO/C-3 h and d) cycling performance of cLTO and LTO/C-3 h at 1 C for 200 cycles.

surface of the LTO. Therefore, preliminary measurements which check the characteristics of the coating for in-line inspection and quality control, such as methods like SRS, are invaluable for cost-effective industrially scaled production. Thus, the quality of surface engineering is more important, as it may have the opposite effect of its intended purpose. Our optimized carbon deposition process resulted in an ultrathin conformal carbon coating layer that significantly suppressed gassing and enhanced rate capability.

Acknowledgements

The authors gratefully acknowledge the financial support from the Ministry of Science and Technology (MOST) in Taiwan (109-3111-8-006-001 and 110-2636-E-006-016). This work was also partially supported by the Hierarchical Green-Energy Materials (Hi-GEM) Research Center, from The Featured Areas Research Center Program within the framework of the Higher Education Sprout Project by the Ministry of Education (MOE) and MOST (110-2634-F-006-017) in Taiwan.

Conflict of Interest

The authors declare no conflict of interest.

Data Availability Statement

The data that support the findings of this study are available from the corresponding author upon reasonable request.

Keywords: carbon coating · gassing · $Li_4Ti_5O_{12}$ · lithium-ion batteries · in operando measurement · cyclic voltammogram

[1] J. Wiebe, THOMSON REUTERS (n.d.).
[2] Y. Ju, R. N. Nasara, C. Lee, Y. Miyahara, T. Abe, K. Miyazaki, *Electrochemistry* **2022**, 64–67.
[3] C. Wang, Z. Wang, D. Zhao, J. Ren, S. Liu, H. Tang, P. Xu, F. Gao, X. Yue, H. Yang, C. Niu, W. Chu, D. Wang, X. Liu, Z. Wang, Y. Wu, Y. Zhang, *ACS Appl. Mater. Interfaces* **2021**, *13*, 55020–55028.
[4] R. Rajagopalan, Y. Tang, X. Ji, C. Jia, H. Wang, *Adv. Funct. Mater.* **2020**, *30*, 1–35.
[5] L. Wang, Z. Wu, M. Jiang, J. Lu, Q. Huang, Y. Zhang, L. Fu, M. Wu, Y. Wu, *J. Mater. Chem. A* **2020**, *8*, 9313–9321.
[6] B. Li, X. Zhang, T. Wang, Z. He, B. Lu, S. Liang, J. Zhou, *Interfacial Engineering Strategy for High-Performance Zn Metal Anodes*, Springer Singapore, **2022**.
[7] Z. Chen, I. Belharouak, Y. K. Sun, K. Amine, *Adv. Funct. Mater.* **2013**, *23*, 959–969.
[8] S. Wang, J. Liu, K. Rafiz, Y. Jin, Y. Li, Y. S. Lin, *J. Electrochem. Soc.* **2019**, *166*, A4150–A4157.
[9] W. Liu, H. Liu, Q. Wang, J. Zhang, B. Xia, G. Min, *J. Power Sources* **2017**, *369*, 103–110.
[10] J. Liu, P. Bian, J. Li, W. Ji, H. Hao, A. Yu, *J. Power Sources* **2015**, *286*, 380–387.

[11] E. Pohjalainen, J. Kallioinen, T. Kallio, *J. Power Sources* **2015**, *279*, 481–486.
[12] K. Wu, J. Yang, Y. Liu, Y. Zhang, C. Wang, J. Xu, F. Ning, D. Wang, *J. Power Sources* **2013**, *237*, 285–290.
[13] C. R. Fell, L. Sun, P. B. Hallac, B. Metz, B. Sisk, *J. Electrochem. Soc.* **2015**, *162*, A1916–A1920.
[14] S. J. An, J. Li, C. Daniel, D. Mohanty, S. Nagpure, D. L. Wood, *Carbon* **2016**, *105*, 52–76.
[15] S. Wang, K. Yang, F. Gao, D. Wang, C. Shen, *RSC Adv.* **2016**, *6*, 77105–77110.
[16] Y. B. He, B. Li, M. Liu, C. Zhang, W. Lv, C. Yang, J. Li, H. Du, B. Zhang, Q. H. Yang, J. K. Kim, F. Kang, *Sci. Rep.* **2012**, *2*, 33–35.
[17] R. Bernhard, S. Meini, H. A. Gasteiger, *J. Electrochem. Soc.* **2014**, *161*, A497–A505.
[18] Y. Qin, Z. Chen, I. Belharouak, K. A. Pi, USDOE Argonne Rep. **2011**.
[19] W. Lv, J. Gu, Y. Niu, K. Wen, W. He, *J. Electrochem. Soc.* **2017**, *164*, A2213–A2224.
[20] K. Wu, J. Yang, X. Y. Qiu, J. M. Xu, Q. Q. Zhang, J. Jin, Q. C. Zhuang, *Electrochim. Acta* **2013**, *108*, 841–851.
[21] M. He, E. Castel, A. Laumann, G. Nuspl, P. Novák, E. J. Berg, *J. Electrochem. Soc.* **2015**, *162*, A870–A876.
[22] M. Metzger, B. Strehle, S. Solchenbach, H. A. Gasteiger, *J. Electrochem. Soc.* **2016**, *163*, A798–A809.
[23] L. Wen, Z. Wu, H. Luo, R. Song, F. Li, *J. Electrochem. Soc.* **2015**, *162*, A3038–A3044.
[24] C. Han, Y. B. He, H. Li, B. Li, H. Du, X. Qin, F. Kang, *Electrochim. Acta* **2015**, *157*, 266–273.
[25] W. Li, X. Li, M. Chen, Z. Xie, J. Zhang, S. Dong, M. Qu, *Electrochim. Acta* **2014**, *139*, 104–110.
[26] Q. Lu, J. Fang, J. Yang, X. Feng, J. Wang, Y. Nuli, *RSC Adv.* **2014**, *4*, 10280–10283.
[27] R. Wang, X. Li, B. Zhang, Z. Wang, H. Guo, *J. Alloys Compd.* **2015**, *648*, 512–520.
[28] J. Gao, B. Gong, Q. Zhang, G. Wang, Y. Dai, W. Fan, Ionics (Kiel). **2015**, 21, 2409–2416.
[29] L. F. Shen, X. G. Zhang, E. Uchaker, C. Z. Yuan, G. Cao, *Adv. Energy Mater.* **2012**, *2*, 691–698.
[30] Z. Zhu, F. Cheng, J. Chen, *J. Mater. Chem. A* **2013**, *1*, 9484–9490.
[31] Y. B. He, F. Ning, B. Li, Q. S. Song, W. Lv, H. Du, D. Zhai, F. Su, Q. H. Yang, F. Kang, *J. Power Sources* **2012**, *202*, 253–261.
[32] R. N. Nasara, P. C. Tsai, S. K. Lin, *Adv. Mater. Interfaces* **2017**, *4*, 1–10.
[33] I. Belharouak, G. M. Koenig, T. Tan, H. Yumoto, N. Ota, K. Amine, *J. Electrochem. Soc.* **2012**, *159*, A1165–A1170.
[34] Q. Wang, J. Zhang, W. Liu, X. Xie, B. Xia, *J. Power Sources* **2017**, *343*, 564–570.
[35] J. C. Burns, N. N. Sinha, G. Jain, H. Ye, C. M. VanElzen, E. Scott, A. Xiao, W. M. Lamanna, J. R. Dahn, *J. Electrochem. Soc.* **2014**, *161*, A247–A255.
[36] S. Meini, N. Tsiouvaras, K. U. Schwenke, M. Piana, H. Beyer, L. Lange, H. A. Gasteiger, *Phys. Chem. Chem. Phys.* **2013**, *15*, 11478–11493.
[37] H. Yi, Y. Liu, X. Lu, *Solid State Ionics* **2022**, *375*, 115852.
[38] K. Ariyoshi, T. Ino, Y. Yamada, *J. Power Sources* **2019**, *430*, 150–156.
[39] M. S. Song, A. Benayad, Y. M. Choi, K. S. Park, *Chem. Commun.* **2012**, *48*, 516–518.
[40] A. Vasileiadis, N. J. J. de Klerk, R. B. Smith, S. Ganapathy, P. P. R. M. L. Harks, M. Z. Bazant, M. Wagemaker, *Adv. Funct. Mater.* **2018**, *28*, 1–18.
[41] M. Kitta, T. Akita, S. Tanaka, M. Kohyama, *J. Power Sources* **2013**, *237*, 26–32.
[42] K. Mukai, T. Nonaka, T. Uyama, *Energy Storage Mater.* **2022**, *44*, 547–556.
[43] M. Kitta, T. Matsuda, Y. Maeda, T. Akita, S. Tanaka, Y. Kido, M. Kohyama, *Surf. Sci.* **2014**, *619*, 5–9.
[44] X. Lu, L. Gu, Y. S. Hu, H. C. Chiu, H. Li, G. P. Demopoulos, L. Chen, *J. Am. Chem. Soc.* **2015** 137, 1581–1586.
[45] Y. B. He, M. Liu, Z. D. Huang, B. Zhang, Y. Yu, B. Li, F. Kang, J. K. Kim, *J. Power Sources* **2013**, *239*, 269–276.
[46] T. Liu, X. Li, S. Sun, X. Sun, F. Cao, T. Ohsaka, J. Wu, *Electrochim. Acta* **2018**, *269*, 422–428.
[47] M. S. Song, R. H. Kim, S. W. Baek, K. S. Lee, K. Park, A. Benayad, *J. Mater. Chem. A* **2014**, *2*, 631–636.
[48] X. Guo, H. F. Xiang, T. P. Zhou, W. H. Li, X. W. Wang, J. X. Zhou, Y. Yu, *Electrochim. Acta* **2013**, *109*, 33–38.
[49] I. Belharouak, Y.-K. Sun, W. Lu, K. Amine, *J. Electrochem. Soc.* **2007**, *154*, A1083.
[50] D. V. Pelegov, R. N. Nasara, C. H. Tu, S. K. Lin, *Phys. Chem. Chem. Phys.* **2019**, *21*, 20757–20763.
[51] G. Yang, S. J. Park, *Sci. Rep.* **2019**, *9*, 1–9.
[52] D. V. Pelegov, A. A. Koshkina, B. N. Slautin, V. S. Gorshkov, *J. Raman Spectrosc.* **2019**, *50*, 1015–1026.
[53] D. V. Pelegov, B. N. Slautin, V. S. Gorshkov, P. S. Zelenovskiy, E. A. Kiselev, A. L. Kholkin, V. Y. Shur, *J. Power Sources* **2017**, *346*, 143–150.
[54] R. N. Nasara, W. Ma, Y. Kondo, K. Miyazaki, Y. Miyahara, T. Fukutsuka, C. Lin, S. Lin, T. Abe, *ChemSusChem* **2020**, *13*, 4041–4050.
[55] S. A. Hong, S. Bin Lee, O. S. Joo, J. W. Kang, B. W. Cho, J. S. Lim, *J. Mater. Sci.* **2016**, *51*, 6220–6234.
[56] Y. Wang, W. Zou, X. Dai, L. Feng, H. Zhang, A. Zhou, J. Li, *Ionics (Kiel)* **2014**, **20**, 1377–1383.

Manuscript received: January 4, 2021
Revised manuscript received: February 11, 2022
Accepted manuscript online: February 16, 2022